

# The effect of plaque morphology, material composition and microcalcifications on the risk of cap rupture: A structural analysis of vulnerable atherosclerotic plaques

- 1 Andrea Corti<sup>1</sup>, Annalisa De Paolis<sup>1</sup>, Pnina Grossman<sup>1</sup>, Phuc A. Dinh<sup>1</sup>, Elena Aikawa<sup>2,†</sup>, Sheldon
- 2 Weinbaum<sup>1,†</sup>, Luis Cardoso<sup>1,†,\*</sup>
- 3 <sup>1</sup>City College of the City University of New York, Department of Biomedical Engineering, New
- 4 York, NY 10029, USA
- 5 <sup>2</sup>Department of Medicine, Brigham and Women's Hospital, Harvard Medical School, Boston, MA
- 6 02115, USA
- 7 †These authors contributed equally to this work
- **8** \* Correspondence:
- 9 Luis Cardoso
- 10 cardoso@ccny.cuny.edu
- 11 Words: **5675**
- 12 Figures: 7
- 13 Keywords: Plaque rupture, microcalcifications, acute coronary events, cap thickness, remodeling
- 14 index, numerical modeling, vulnerable plaque
- 15 Abstract

22

23

24

25

26

27

28

29

30

31

- Background: The mechanical rupture of an atheroma cap may initiate a thrombus formation, followed by an acute coronary event and death. Several morphology and tissue composition factors have been identified to play a role on the mechanical stability of an atheroma, including cap thickness, lipid core stiffness, remodeling index, and blood pressure. More recently, the presence of microcalcifications (μCalcs) in the atheroma cap has been demonstrated, but their combined effect with other vulnerability factors has not been fully investigated.
  - **Methods:** We performed numerical simulations on 3D idealized lesions and a microCT-derived human coronary atheroma, to quantitatively analyze the atheroma cap rupture. From the predicted cap stresses, we defined a biomechanics-based vulnerability index (VI) to classify the impact of each risk factor on plaque stability, and developed a predictive model based on their synergistic effect.
  - **Results:** Plaques with low remodeling index and soft lipid cores exhibit higher VI and can shift the location of maximal wall stresses. The VI exponentially rises as the cap becomes thinner, while presence of a  $\mu$ Calc causes an additional 2.5-fold increase in vulnerability for a spherical inclusion. The human coronary atheroma model had a stable phenotype, but it was transformed into a vulnerable plaque after introducing a single spherical  $\mu$ Calc in its cap. Overall, cap thickness and  $\mu$ Calcs are the two most influential factors of mechanical rupture risk.
- 32 **Conclusions:** Our findings provide supporting evidence that high risk lesions are non-obstructive plaques with softer (lipid-rich) cores and a thin cap with  $\mu$ Calcs. However, stable plaques may still rupture in the presence of  $\mu$ Calcs.

#### 1 Introduction

35

36

37

38

39

40

41 42

43

44

45 46

47

48 49

50

51

52

53

54

55

56

57

58

59

60 61

62

63

64

65

66

67

68

69

70

71

72

73

74

75

76 77

78

79

The vulnerable patient concept (1,2) refers to individuals at increased risk of suffering an acute coronary event, i.e., patients with high atherosclerotic burden, presence of one or several vulnerable plaques, endothelial injury or dysfunction due to clinical risk factors (3). Plaque rupture, plaque erosion and calcified nodules (4–6) are the three most important vulnerable plaque phenotypes that are linked to coronary thrombosis and acute coronary events (3). The plaque rupture (7) is characterized by a thin fibrous cap measuring <65µm thickness over a lipid-rich or necrotic core; where the cap is infiltrated by macrophages and other inflammatory cells, apoptotic cells, lipids, neovessels and intraplaque hemorrhage(8-12). In some cases, the ruptured atheroma may heal and contribute to the increase of atheroma volume, stenosis, and subsequent rupture(s) that may be responsible for acute coronary events. In turn, plaque erosion is characterized by denudation of the coronary artery endothelium (5),(13) and the plaque calcified nodules consist of mineralized tissue present at the neointima layer of the vessel, that comes in contact with the arterial blood flow (5). Patients that develop acute coronary events also exhibit vulnerable blood and vulnerable myocardium. Vulnerable blood has an increased thrombotic potential, which could lead to thrombosis in fibrotic and severely stenotic plaques (3). Vulnerable myocardium refers to functional coronary alterations and hemodynamic changes (2) such as stasis, non-laminar blood flow, endothelial injury or dysfunction (3). It is now accepted that the pathophysiology of an acute coronary event involve patients with vulnerable blood, myocardium and plaque rupture/erosion, and that their respective contributions in isolation are inadequate to predict coronary events. Nonetheless, the underlying biomechanics of atheroma cap rupture, a major component of acute coronary events, has not been fully elucidated.

The biomechanics of plaque rupture depends on several tissue composition and morphological factors, including the fibrous cap (FC) thickness (14,15), the lipid core material properties and thickness (16), vessel wall tissue properties (17), and the morphology of the lesion (16)(18). The combination of these intrinsic factors, together with the blood pressure (e.g., hypertension), determines the mechanical background stress levels on the cap. When the developed stresses exceed the ultimate tensile strength (UTS) in the circumferential direction of the cap tissue, the cap ruptures and initiates a thrombogenic response that may restrict the blood flow to downstream tissues. Importantly, the role of calcified tissue in vulnerable plaque rupture is not fully understood. On one hand, large calcifications potentially lead to mechanical stabilization of the atheroma. On the other hand, calcified nodules have been shown to initiate a thrombogenic response following a coronary event. While calcium scoring is an indicator of atherosclerotic burden (19–23), in this longstanding cap rupture paradigm, the culprit plaque of an acute coronary event is believed to have a low amount of calcification, when compared with non-ruptured advanced lesions, which show much larger calcium scores (19–23). This paradigm has been challenged since Vengrenyuk et al. first showed in 2006 that there were small cellular size microcalcifications (µCalcs) in thin fibrous caps, and that these inclusions could at least double the local tissue stresses (15–17,19–21,24–30). Indeed, it has been shown using high-resolution micro-CT (HR-μCT) that μCalcs in fibrous caps are not rare but numerous (27,30,31), and that the overall effect of µCalcs in plaque vulnerability can be summarized as an intensifier of the background circumferential stress in the cap, resulting in increased vulnerability (25,29). µCalcs are formed by aggregation of calcifying extracellular vesicles (32) and have been reported at the site of rupture (27). The key concept in the role of µCalcs as a risk factor for vulnerability is that they have to reside in the fibrous cap tissue, where they amplify the background stress and increase the likelihood of rupture. Otherwise, if µCalcs are located in the lipid/necrotic core, they won't affect the biomechanics of the plaque, as they would behave as floating debris.

The purpose of this study was to provide a quantitative analysis of atheroma cap rupture risk using three-dimensional (3D) idealized atherosclerotic coronary plaques under the combined effect of  $\mu$ Calcs with several other known risk factors (i.e. cap thickness, lipid core stiffness, remodeling index, blood pressure). To investigate the individual and synergistic effect of these risk factors to the biomechanics of plaque rupture, a vulnerability index was defined and a nonlinear model was proposed to predict the vulnerability index based on the combined effect of each risk factor. Finally, a stable, non-ruptured human atherosclerotic coronary artery was used to create a model derived from high-resolution microCT images, and tested under normal and hypertensive blood pressure, as well as with and without one  $\mu$ Calc in its cap, to determine the effect of blood pressure and presence of one  $\mu$ Calc on the vulnerability of such atheroma.

#### 2 Materials and Methods

To examine the influence of different biomechanical risk factors on cap stability, we performed numerical simulations on 3D idealized geometries of atherosclerotic arteries with various morphological features, including lipid core material properties and  $\mu$ Calcs in their cap under normal and hypertensive blood pressures. First, we studied the effect of different remodeling indices and lipid core Young's moduli on the cap background stress and the location of highest stresses in the artery. This way, we were able to determine the combinations of plaque morphology traits and material properties that represent the upper and lower limit of cap rupture risk. The most unstable condition was then considered for studying the impact of cap thickness,  $\mu$ Calcs inclusion and blood pressure regime. Finally, the predictive property of our results was tested on the case of a human atherosclerotic coronary artery in the presence and absence of one  $\mu$ Calc and under varying blood pressure levels and lipid core stiffnesses.

#### Anatomical features of arterial models

Idealized atherosclerotic plaque models were conceived to present thickening of the intima layer (33) and an eccentric plaque with remodeling index (RI), degree of stenosis and lumen reduction in agreement with Glagov's morphological and mathematical description of lesion growth (16,18) (see Appendix, Section1A, Eq. I, II, III). The values of each anatomical feature for all models are reported in Table1. In this study, we covered RI values of 1.25 (asymptomatic plaque with minimal lumen occlusion), 1.4 (moderate stenosis) and 1.6 (symptomatic critical stenosis) (Fig1A). The fibrous cap (FC) thickness values that we considered were of 50, 100, 150 and 200 μm (Fig1B), and were obtained by increasing the core thickness towards the cap proper.

RI	Stenosis (lumen reduction)	Core length (mm)			
1.25	50% (10%)	7.4			
1.4	62% (23%)	7.8			
1.6	80% (50%)	8.2			

Table 1. List of the remodeling indices considered in this study with their respective degrees of stenosis, luminal occlusion and lipid core length.

The human model (**Fig1C**) represents a segment of the left anterior descending coronary artery dissected from a fresh heart obtained from The National Disease Research Interchange (recovered < 6h post mortem) with myocardial infarction, and IT was part of the data set studied in (30). The sample was scanned with  $6.7\mu m$  high-resolution microcomputed tomography (HR- $\mu$ CT) as described in the

Appendix, Section 1A. The plaque consists of an 8.45mm-long lipid core with a minimum fibrous cap thickness of 125 $\mu$ m. The sample presents a remodeling index of 1.29 with a degree of stenosis of 61% that causes a 31% luminal occlusion. This atheroma exhibits the typical morphological traits of a vulnerable plaque, except for the thickness of its cap. Compared to the idealized models with RI of 1.25 and 1.4, the human sample contains a thicker core of 1.1mm. However, the relative core thickness with respect to the whole plaque is 66%, which is similar to the 72% and 65% in the idealized geometries with 100 $\mu$ m- and 150 $\mu$ m-thick caps and 1.25 remodeling index. The  $\mu$ Calc was designed to represent a single solid calcified particle of spherical profile with a diameter of 15 $\mu$ m and was placed at the center of the FC.

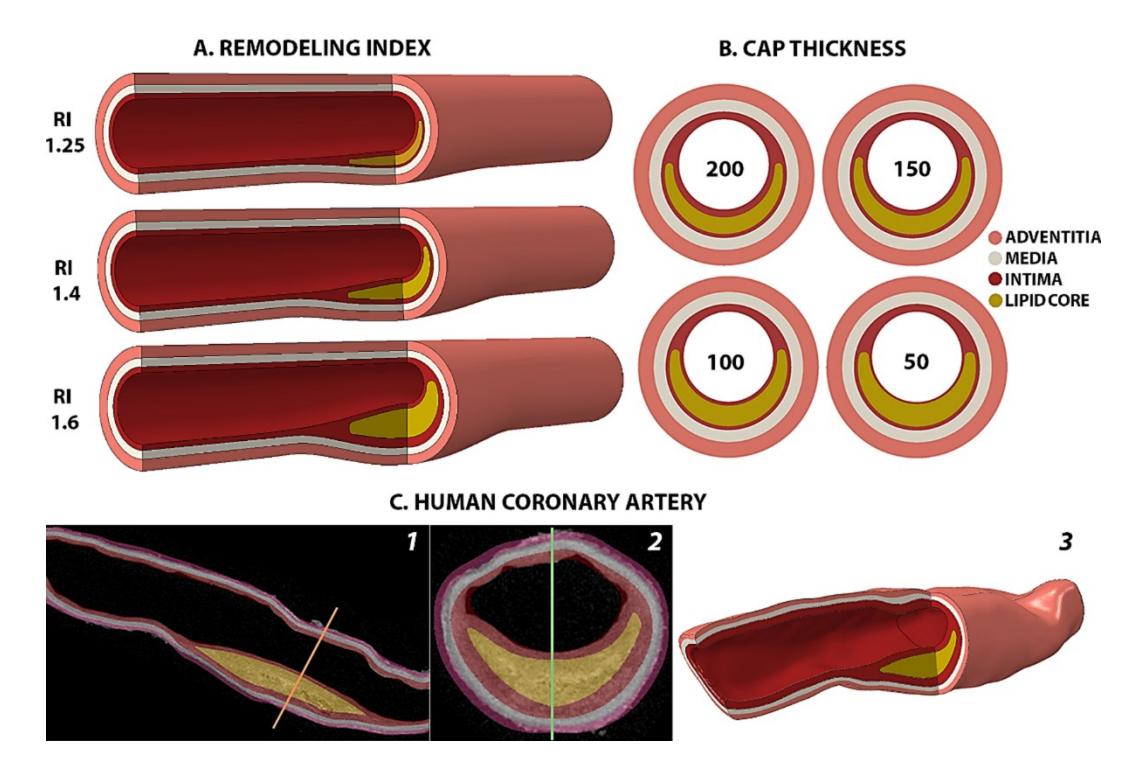


Figure 1. Representation of the arterial models analyzed. (A) Isometric view of the idealized geometries of human coronary arteries with different remodeling indices and a 200 $\mu$ m-thick fibrous cap. (B) Cross section of fibroatheromas with different cap thicknesses of 200, 150, 100 and 50 $\mu$ m for the case of RI=1.25. (C) Rendering of the human coronary artery from 2D HR- $\mu$ CT images in sagittal (1) and coronal (2) views to the 3D geometry reconstruction (3).

#### Material Properties

The arterial wall vessel layers were considered as anisotropic and homogeneous. Their material properties were defined by the Holzapfel-Gasser-Ogden (HGO) hyperelastic constitutive model (34),(35) which takes into consideration the collagenous fiber orientation in the tissue. To reproduce the tissue rupture mechanism, we coupled the hyperelastic failure description proposed by Volokh et al. (36) to the HGO model of the intimal layer. The damage model was fit to not alter the stress-strain response of the intima from that reported by Holzapfel et al. and to trigger tissue rupture at an average Principal Stress of 545kPa (14). A detailed description of the model definition and layer-specific material properties are provided in the **Appendix**, **Section 1**. The lipid core was considered as an

A. Blood pressure waves

—healthy —hypertensive

200

160

80

142 isotropic, almost incompressible, elastic material with Young's modulus ( $E_{core}$ ) of 5, 25 and 50kPa and 143

Poisson's ratio (v) of 0.49 (15). The µCalcs were modeled with properties similar to calcified bone

tissue, with  $E_{calc} = 18$  GPa and v = 0.3 (37).

145

146

147

148

149

150

151

152

153

154

155

156

157

158

159 160

161

162

163

164

165

166

167

168

169

170

171

172

173 174

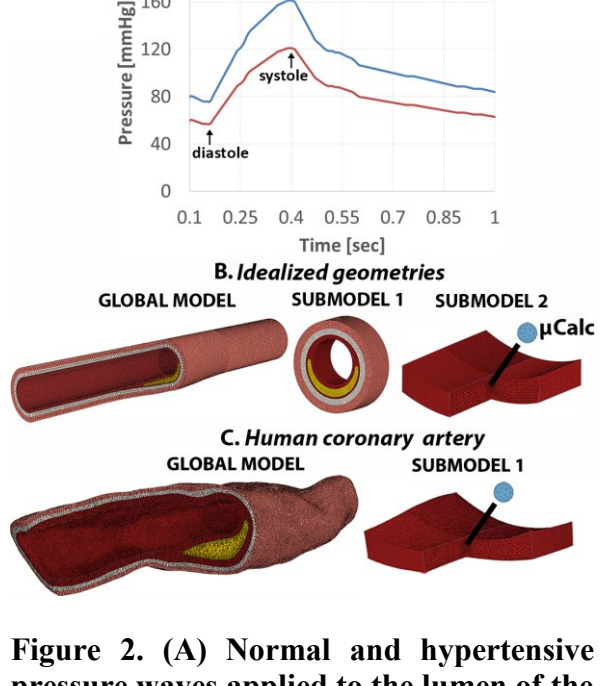
144

#### Boundary conditions and Loadings

Two blood flow regimes were considered in this study (Fig2A). The first one represents a normal pressure wave of 120/60mmHg extracted from patient-based coronary measurement (24). The second case resembles a stage 2 hypertensive condition with a blood pressure of 160/90mmHg and was obtained by amplifying the normal pressure wave. The two axial ends of the artery were free to move in the radial direction only, reflecting the constraint from the artery to tissue tethering. To maximize the accuracy of the cap stress calculation we implemented a sub-modeling approach (Fig2B) described in detail in the Appendix, Section1C. A total of 51 finite element simulations were performed Abagus in (Abagus/CAE, Dassault Systemes, v.2019).

#### 3 **Results**

The goal of this parametric analysis was to determine the relative effect of morphological and tissue composition risk factors on the atheroma cap rupture. In this section, we first present a qualitative overview of the location of maximal wall stresses as a function of plaque morphology and material properties. Then, we provide a quantitative description of peak cap stresses (PCS) and cap rupture by simulating tissue failure and deriving a biomechanical vulnerability index (VI) for each



pressure waves applied to the lumen of the artery to replicate blood flow on 1-second time span. Mesh view of the global model and subsequent submodels of the idealized geometries (B) and human coronary sample (C)

risk factor. This non-dimensional coefficient was defined as:

$$VI = \frac{PCS [MPa]}{Ultimate \ tensile \ stresss \ [MPa]}$$
(11)

175 176

177 178

180

where the PCS is the average cap stress obtained considering 30 mesh elements in the region of highest principal stresses in the cap, and the ultimate tensile stress is the threshold stress for rupture (545kPa)

reported in the literature (14,15). The structure-function relationship between each risk factor and the

179 vulnerability index was analyzed by obtaining the Spearman's correlation coefficient (ρ) followed by

two-tailed t-test to quantify the strength of correlation (MatLab, Mathworks, v.R2022a). To describe

- the combined effect of all the risk factors on plaque vulnerability, we derived a multi-variable
- predictive model based on a stepwise non-linear regression analysis. The null hypothesis was rejected
- 183 if p-value < 0.05.

## 3.1 Role of remodeling index, lipid core material properties and cap thickness on atheroma background stresses

In order to investigate the relative importance of the different predictor variables on the atheroma background stresses and vulnerability index, we studied 3 remodeling indices, 3 lipid core Young's moduli and 3 cap thicknesses. The effect of the remodeling index was analyzed while keeping a constant  $E_{core}$  of 5kPa. On the other hand, varying  $E_{core}$  values were examined in the case of RI = 1.25. Every case was further combined with 3 different cap thicknesses of 200, 100 and 50µm under normal blood pressure (120/60mmHg). In addition, we included in the analysis the phenotype with RI = 1.6 and  $E_{core}$  = 50kPa, for all three cap thicknesses, as it represents the most stable condition, for a total of 18 cases investigated (Fig3).

Our results show that greater remodeling indices and stiffer lipid cores correspond to lower cap stresses and thus more stable plaques. Conversely, atheroma with low remodeling index and soft lipid core results in higher cap stresses. Also, it was observed that both the remodeling index and lipid core properties can shift the location of highest stresses from the atheroma cap region to outside the atheroma, at the proximal and distal sides of the artery. Thus, the maximal principal stresses does not occur at the atheroma when the remodeling index is high and the lipid core is stiff. This phenomenon is especially evident when the cap is 200 or  $100\mu m$  thick, in which case a higher degree of stenosis or core stiffness yields to atheroma cap stresses that are lower than the stresses in healthy regions of the blood vessel. Interestingly, if the background stress in the atheroma is low, such as the case when RI = 1.6 and  $E_{core} = 50 kPa$ , even a  $50 \mu m$ -thick cap appears to experience PCS levels that are far below the threshold for rupture and the cap stresses are lower than those at proximal/distal luminal areas of the vessel. Thus, atheroma characterized by soft lipid core (i.e.,  $E_{core} = 5 kPa$ ) and low remodeling index values (i.e., RI = 1.25), which are typical of early stage plaques, induce the highest stresses in the cap proper, while more advanced plaques, exhibiting greater remodeling index (RI > 1.6), become mostly stable.

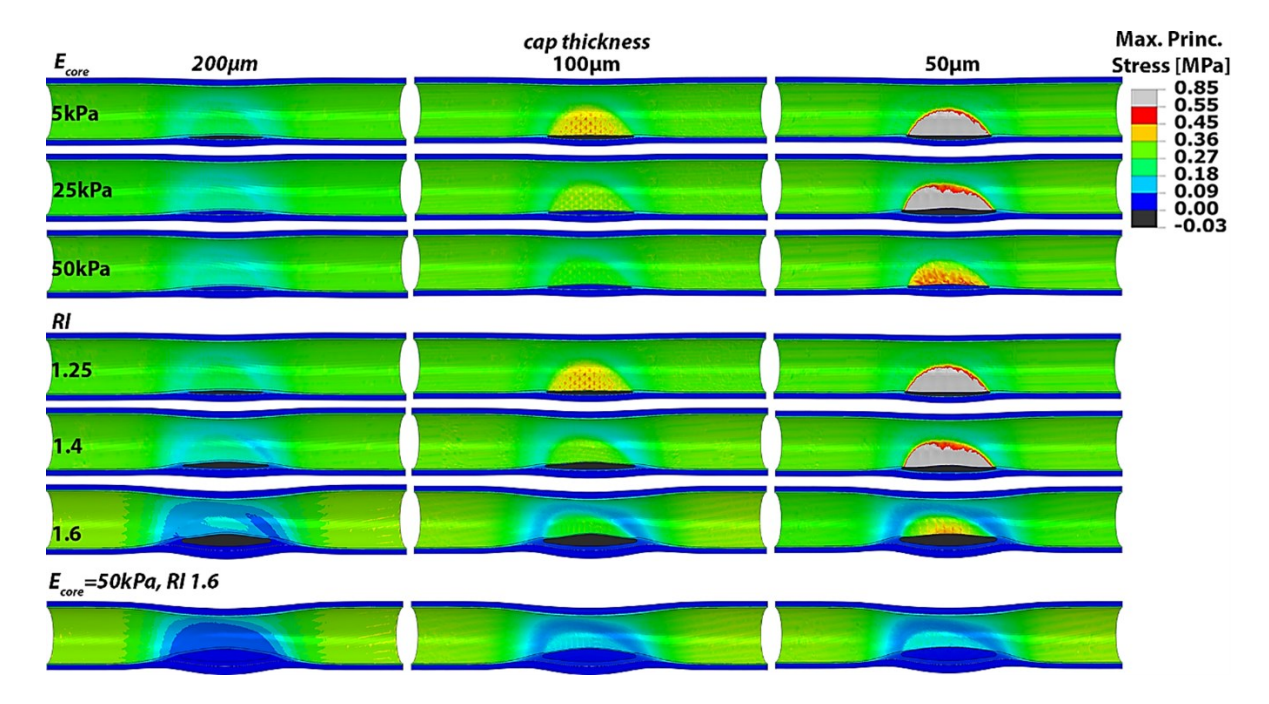


Figure 3. Longitudinal cut of idealized models with varying RI, Ecore and cap thickness showing the Max Principal Stress distributions. Higher remodeling indices and stiffer lipid cores clearly influence the PCS and the location of highest wall stress.

These observations are supported by the biomechanical vulnerability index obtained for each phenotype (**Fig4**). Plaques with 50µm-thick FC reach threshold for rupture except when  $E_{core} = 50 kPa$  or RI = 1.6, suggesting that the stability of very thin caps can increase under certain plaque morphologies and lipid core stiffness. All other cases exhibit VI < 1, indicating that tissue failure would not occur in these circumstances. **Figure 4** also shows the significant impact of cap thickness on plaque vulnerability, with an exponential increase in stresses as the cap becomes thinner. For the same RI and  $E_{core}$ , a 50µm-cap experiences more than 5-fold increase in PCS levels compared to a 200µm-thick cap. Statistical analysis of Spearman's correlation coefficient among remodeling index, lipid core stiffness, cap thickness and vulnerability index indicates that the strongest relationship exist between the cap thickness and the vulnerability index,  $\rho_{CT-VI}$  = -0.62 with  $p_{CT-VI}$  = 4.85E-04. A weaker effect of RI and Ecore on the vulnerability index was observed,  $\rho_{RI-VI}$  = -0.38 and  $\rho_{Ecore-VI}$  = -0.35, respectively, with p-values  $p_{RI-VI}$  = 0.049 and  $p_{Ecore-VI}$  = 0.0697. Thus, cap thickness is the most influential factor on the behavior of the vulnerability index among the analyzed parameters.

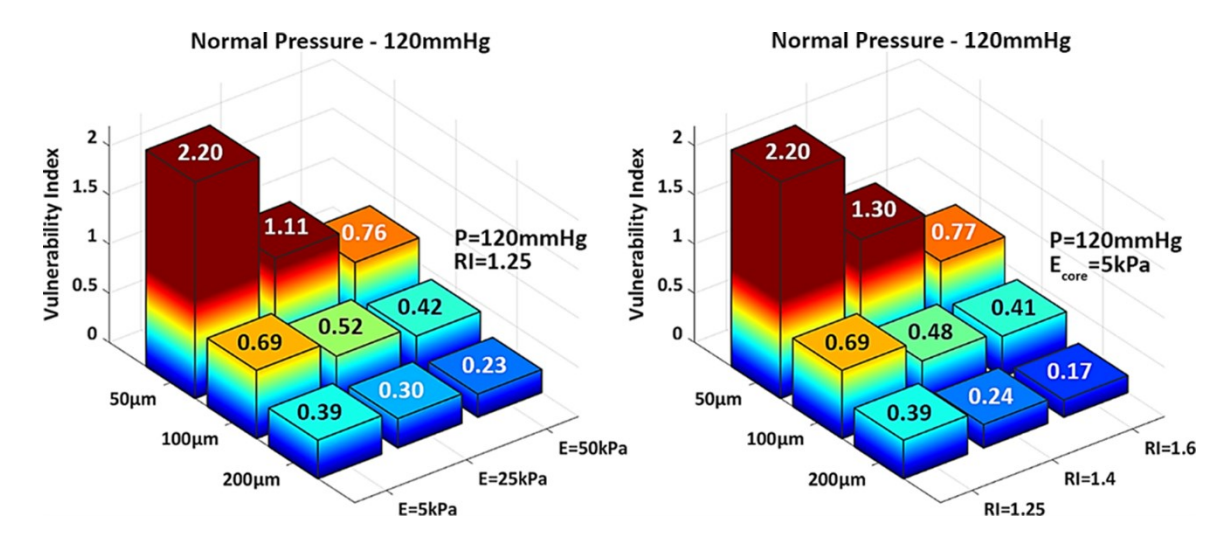


Figure 4. 3D-barplots of the change of the vulnerability index based on cap thickness, lipid core Young's Modulus (Left) and remodeling index (Right). The exact VI value is reported on top of every bar.

#### 3.2 Role of cap thickness, blood pressure and µCalcs in caps on atheroma vulnerability index

The impact of cap thickness analyzed in the previous section was further investigated under the action of normal and hypertensive pressures and for the case of one spherical  $\mu$ Calc embedded in the cap tissue, using a tissue failure algorithm. The effect of these factors was studied in arteries with RI = 1.25 and  $E_{core} = 5kPa$ , which were shown to lead to the highest atheroma background stress in the previous section.

The tissue failure mechanism and rupture propagation due to the presence of a spherical microcalcification is exemplified in **Figure 5**. The  $\mu$ Calc amplifies the tissue background stresses by a factor of about 2.5 at its tensile poles. In the presence of a  $\mu$ Calc, the rupture mechanism is driven by stress concentrations at the tensile poles of the calcification (**Fig5**) while the background stresses in the cap tissue (e.g. 216kPa in **Figure 5**) is way below the ultimate tensile stress threshold for rupture (545kPa). When the stresses at the  $\mu$ Calc poles exceed the ultimate tensile stress threshold for rupture, tissue rupture initiates as small voids around the  $\mu$ Calc, which then explosively grows through the thickness of the cap, ultimately exposing the underlying core to the flowing blood. Comparison of the stress-strain response of a 100 $\mu$ m cap with and without one spherical  $\mu$ Calc, under the same systolic pressure is shown in the right hand side panel in **Figure 5**.

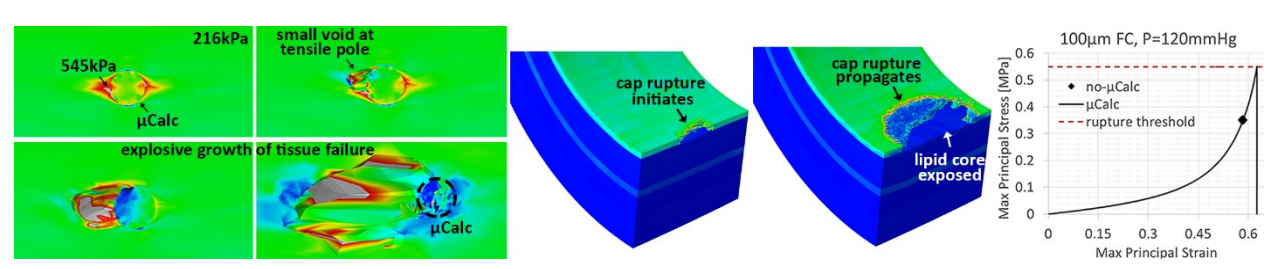


Figure 5. Illustration of the tissue failure mechanism and rupture propagation due to the presence of a spherical micro-calcification. (Left) The  $\mu$ Calc amplifies the tissue background stresses by a factor of about 2.5 at its tensile poles. When these stresses exceed the threshold for

rupture, small voids start forming in these regions. If the tissue continues to stretch, the voids grow explosively through the tissue. (Center) Cap rupture initiates as a small fissuring at the luminal side and then propagates as the tissue is more exerted, until exposing the underlying lipid core. (Right) Comparison of the stress-strain response of a  $100\mu m$  cap with and without one spherical  $\mu Calc$ , under the same systolic pressure.

The results of this analysis confirm the substantial influence of cap thinning on PCS levels and vulnerability index. In the absence of a  $\mu$ Calc, the 50 $\mu$ m thick cap is the only phenotype that ruptures under normal pressure levels, where the vulnerability index exceeds more than two times the threshold for failure (**Fig6 left**). In the case of hypertension however, the 100 $\mu$ m cap also undergoes rupture, with a vulnerability index that is 30% higher than under healthy systolic pressure (**Fig6 right**). However, a significant increase in vulnerability index is observed in all cases after a  $\mu$ Calc was introduced in the atheroma cap. Each phenotype that was considered mechanically stable (i.e. thick caps under normal or hypertensive blood pressure), became vulnerable and reached rupture when a  $\mu$ Calc was introduced in the cap (**Fig6**).

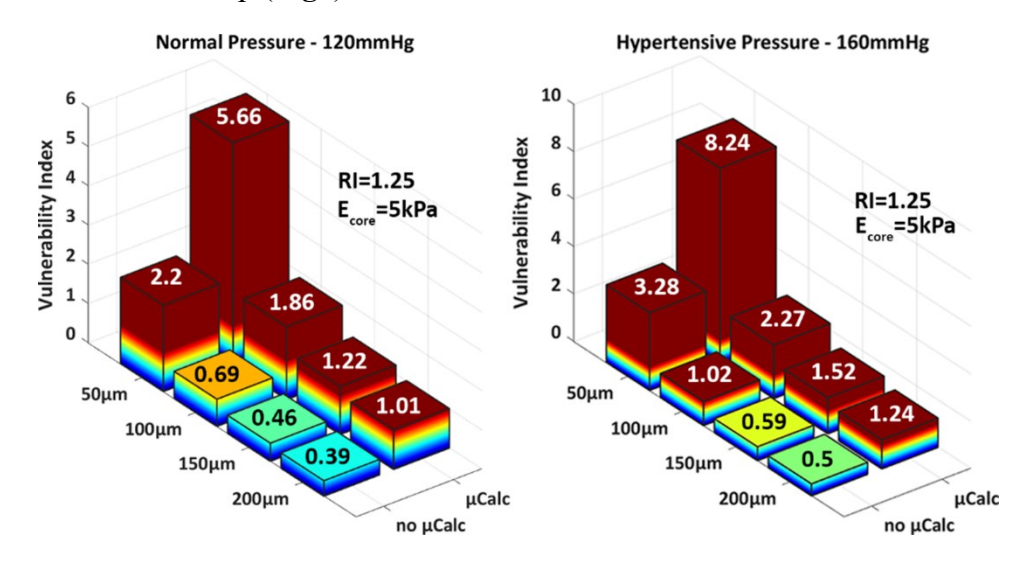


Figure 6. 3D-barplots of the change of the vulnerability index based on cap thickness, the presence of a spherical  $\mu$ Calcs at the center of the cap and blood pressure.

Statistical analysis of these results indicates that the cap thickness ( $\rho_{CT-VI}$  = -0.62 with  $p_{CT-VI}$  = 4.85E-04) and the presence of a  $\mu$ Calc in the cap ( $\rho_{\mu Calc-VI}$  = 0.61 and  $p_{\mu Calc-VI}$  = 6.17E-04) have equally strong impact on cap stability. Indeed, one  $\mu$ Calc in the fibrous cap causes a 2.5-fold increase in the vulnerability index, regardless of cap thickness or peak systolic pressure. The blood pressure also exhibits a significant influence on the vulnerability index, with  $\rho_{BP-VI}$  = 0.43 and  $p_{BP-VI}$  = 0.02. A model capable of predicting the vulnerability index as a function of all the risk factors considered in this study was designed using regression analysis (MatLab, Mathworks, v.R2022a). The nonlinear model was obtained by first considering the intrinsic components that determine the cap background stress (i.e cap thickness, remodeling index and core stiffness) and deriving a generalized stepwise quadratic model. Then, this model is multiplied by a factor that depends on the blood pressure and the  $\mu$ Calc binary variable:

$$VI = f(CT, RI, Ecore, BP, uCalc) = (12)$$

$$(b_1 + b_2CT + b_3RI + b_4Ecore + b_5CT * RI + b_6CT * Ecore + b_7CT^2) * (b_8BP) * (1 + b_9uCalc)$$

- with coefficients:  $b_1 = 7.863$ ,  $b_2 = -0.052$ ,  $b_3 = -3.688$ ,  $b_4 = -0.031$ ,  $b_5 = 0.017$ ,  $b_6 = 1.537$ e-4,  $b_7 = 0.031$
- 7.830e-5,  $b_8 = 9.972e-3$ ,  $b_9=1.5$ . The model shows a strong Spearman correlation coefficient  $\rho=0.967$
- (p=5.359e-8) with the VIs measured from the FEM simulations. This analysis was preferred to a
- 283 linear Pearson analysis as the model's residuals are not normality distributed, based on a
- 284 Kolmogorov-Smirnov test.

#### 3.3 Human coronary artery

A microCT-derived patient-specific model of a human coronary artery was analyzed under normal and hypertensive blood pressures, with and without one spherical  $\mu$ Calc embedded in its cap. Wall stress distributions show higher stresses in the cap but also in other luminal regions (**Fig7A**). The latter case is likely the result of the original shape of the sample, which presented a non-circular lumen profile. Peak cap stresses at systolic pressures are close to values measured in the idealized case with 150 $\mu$ m cap and RI = 1.25. Our results show that the fibrous cap does not rupture under normal nor hypertensive pressure in the absence of the  $\mu$ Calc. Conversely, the presence of the  $\mu$ Calc amplifies the local stresses in the cap, causing the plaque to reach failure under both regimes of pressure, with rupture of the cap tissue occurring around 80mmHg and quickly propagating through the tissue, as shown in **Figure 7B**.

The predictive power of our statistical model was tested against the vulnerability indices computed in numerical simulations of the human coronary at 5 different blood pressures (80, 100, 120, 140, 160mmHg) and 5 lipid core Young's Moduli (5, 15, 25, 35, 50kPa) (Fig7C). Our results indicate that the model is capable of accurately predicting the VI for 9 out of 10 conditions considered. The only phenotype where the vulnerability index was significantly under-predicted is the plaque with Ecore = 50kPa. Nonetheless, the model showed a 100% accuracy at distinguishing vulnerable from stable atheromas (i.e VI<1 or VI>1).

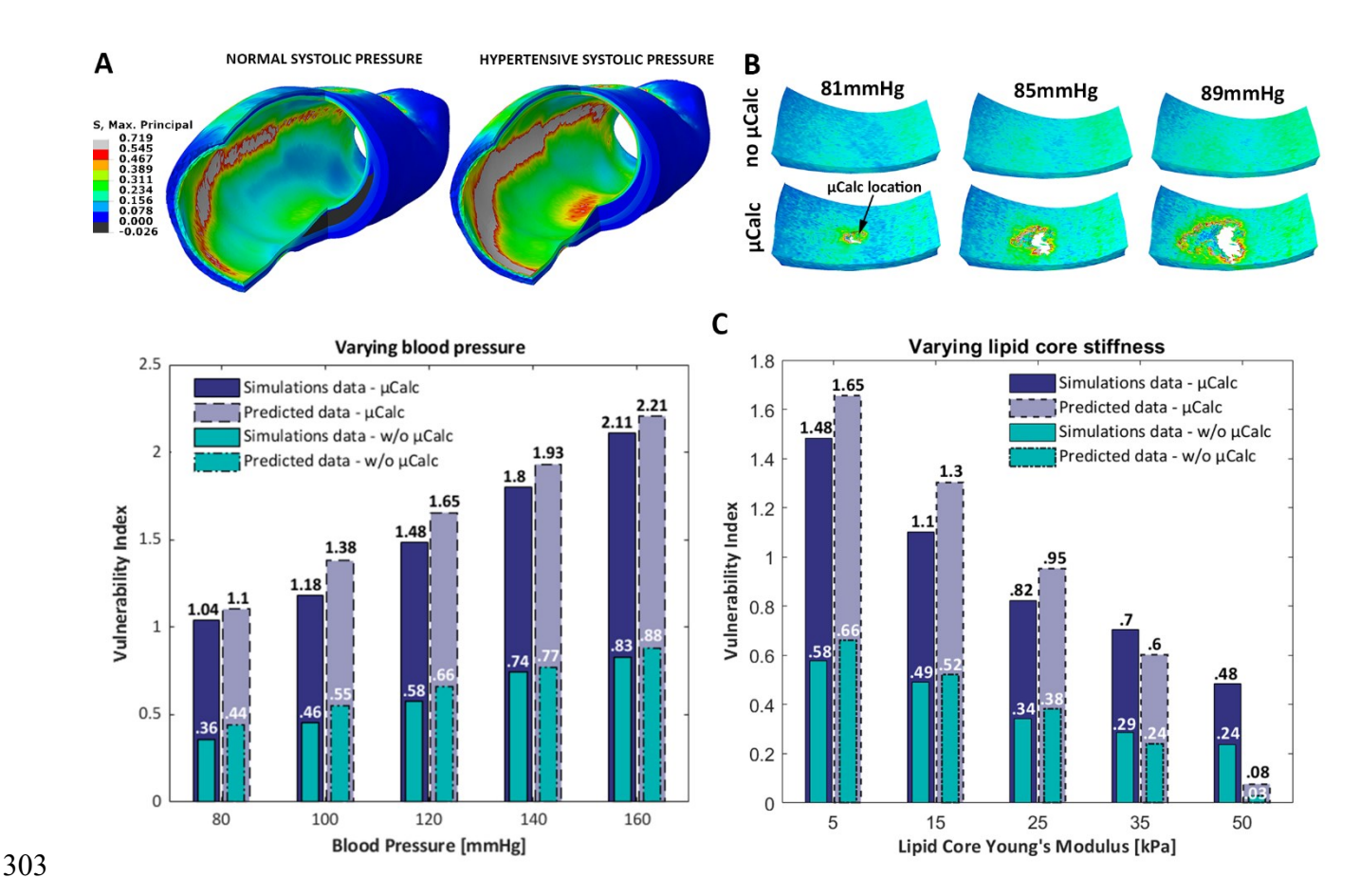


Figure 7. (A) Isometric view of the Maximal Principal Stress distributions on the human coronary under normal and hypertensive blood pressure; (B) sequence of the cap segment submodel with and without the  $\mu$ Calc. In the presence of the  $\mu$ Calc, the cap rupture extensively, starting at the location of the  $\mu$ Calc; (B) 3D-barplot of the change of the vulnerability index for different blood pressures, lipid core stiffness and the presence of one spherical  $\mu$ Calc from FEM analyses and predicted by the statistical model.

#### 4 Discussion

 In the present study, we investigated the contribution of several major biomechanical factors (i.e. cap thickness, lipid core stiffness, remodeling index, blood pressure, and the presence of a  $\mu$ Calc in the cap tissue) to plaque vulnerability using 3D finite element models. A vulnerability index was defined based on the ratio of maximal stresses and the ultimate tensile stress in the cap tissue. The two most significant factors were identified and a non-linear model combining these factors was obtained. The approach was also used to analyze a human atherosclerotic coronary artery model derived from high-resolution microCT images, under normal and hypertensive blood pressure, as well as with and without one  $\mu$ Calc in its cap.

Overall, the presence of a  $\mu$ Calc in the FC and a thin cap compromise the plaque mechanical stability to the greatest extent. We demonstrated that one spherical  $\mu$ Calc amplifies the background stress in the tissue by a factor of 2.5. These findings agree with previous observations from analytical and numerical analyses that reported 2-fold increase in interfacial stresses at the  $\mu$ Calc poles (25,26). Although one spherical  $\mu$ Calc already exhibits a severe effect on plaque vulnerability, other studies have shown that  $\mu$ Calcs can cause up to a 7-fold increase in local tissue stresses, depending on their shape and proximity. Vengrenyuk et al. (38) found that  $\mu$ Calcs with a prolate ellipsoidal configuration

could lead to more than a 4-fold increase in stress at their poles, when aligned along the tensile axis.

Additionally, Kelly-Arnold et al. (27) calculated the stress concentration factor between closely spaced μCalcs and reported a 7-fold increase in stresses when the ratio of the gap between two μCalcs and their diameter is lower than 0.4, if the particles are aligned with the tensile axis. In this study, we demonstrated that one spherical μCalcs is the strongest predictor of cap rupture among other major risk factors. However, μCalcs clusters or ellipsoidal particles could have even more drastic consequences (19,25,27,29).

A fundamental difference between the present study and Kelly-Arnold et al (27) is that in the former study nearly 35,000  $\mu$ Calcs were examined in 22 caps of 66 atheroma that had not ruptured. With an average of more than 1500  $\mu$ Calcs in each cap how was it possible that so many  $\mu$ Calcs could exist in a cap and still not cause an acute coronary event. The answer to this is that the background stress in all these caps was far below the 545 kPa threshold. Indeed, 193  $\mu$ Calc pairs were observed with a spacing that was less than one  $\mu$ Calc diameter and a few were as close 0.5 diameters where the local increase in stress could be 5-fold or higher in the intervening space. Analysis of all these  $\mu$ Calc pairs showed that in no case was the 545 kPa threshold exceeded. While  $\mu$ Calcs greatly increase the risk of rupture, most fortunately, they must also reside at a location where the background tissue stress is high enough to promote plaque rupture.

The other most significant contributor to plaque vulnerability is the cap thickness. Our results show an exponential increase in peak cap stress as the cap becomes thinner, with 50µm-thick caps that are significantly more vulnerable than thicker caps of 100-200µm. These observations correlate well with previous data of 2D and 3D numerical studies (15),(39). Finet et al. (15) demonstrated that fibrous caps thinner than 62µm induced a peak circumferential stress greater than 300kPa, supporting previous histological observations that reported a critical thickness for rupture of 65µm (40). Thin caps have been a widely accepted indicator of plaque instability (41) as they exhibit higher local stresses and have been observed in pathological studies of ruptured plaques (40),(5). However, there is also evidence of non-ruptured plaques with thin caps (5) as well as caps thicker than 100µm that ruptured under exertion(42).

Our results capture well the influence of the core material properties and plaque remodeling on the cap stress levels. We showed that softer cores and a low remodeling index correlate with higher peak cap stresses and plaque vulnerability, in agreement with published data on 2D atherosclerotic arterial models (15),(16),(17). Ohayon et al. (16) performed finite element analyses on 5,500 2D idealized atherosclerotic arteries and showed that plaques are more vulnerable at a low remodeling index, with minimal lumen narrowing. As described by Glagov et al. (18), the early stages of plaque development are characterized by a predominant positive (expansive) remodeling of the artery, with a nearly constant lumen area until a remodeling index of 1.23. Thus, young asymptomatic plaques emerge as the type of lesions at highest risk of rupture. This seems to be supported by in vivo observations in Maehara et al. (44), where the authors examined 300 ruptured coronary plagues detected by intravascular ultrasound. Here, ruptured plaques presented an average remodeling index of  $1.15 \pm 0.28$ , with positive remodeling accounting for 73% of the plaque area. In this study, we also showed that the combination of a high remodeling index with a stiff core can shift the location of maximal stresses from the cap proper to the proximal and distal sides of the artery, outside the atheroma, even when the cap is thinner than the rest of the intima layer. Similar wall stress distributions have been previously reported in numerical simulations on 3D arterial models with high remodeling indices or elevated lumen narrowing (39,42).

Our findings on the effect of plaque morphology and cap thickness are consistent with the parametric analysis performed by Cilla et al. on 3D numerical models (39). Here the authors also studied the significance of varying core length ( $1 \le L \le 8$  mm) and lipid core angle ( $40 \le \alpha \le 88$ ) on the cap stresses. They showed that PCS are not significantly influenced by the core angle and the lipid core length, when the core is longer than 4mm. Based on this knowledge, we believe our idealized 3D models are a comprehensive representation of the most impactful morphological features of the atheroma. Another distinctive driver of wall stresses is high blood pressure. Hypertension leads to increased stretch and vulnerability index even in thicker caps when  $\mu$ Calcs are present, as our results show for the case of a 200 $\mu$ m cap. Additionally, phenotypes without  $\mu$ Calcs and a thick cap (100 $\mu$ m) could still reach rupture, as shown in our analysis and observed in *in-vivo* studies (42)

Finally, the results obtained from the human coronary artery simulations compares well with parametric analyses on idealized models. In particular, the human geometry compares closely to the idealized case of a 150 $\mu$ m cap with RI = 1.25. These models experience similar PCS levels under normal and hypertensive blood pressure (PCS<sub>human</sub>=236-375kPa, PCS<sub>ideal</sub>=252-322kPa) and don't undergo rupture in the absence of  $\mu$ Calcs. Conversely, when the  $\mu$ Calc is introduced in the cap tissue, plaque rupture occurs under both pressure regimes. These findings confirm the fact that the human plaque sample was intact, as we didn't notice any calcified particle in the HR- $\mu$ CT images. As opposed to the idealized case, the human model experiences the maximal wall stresses on non-stenotic regions at the location of high lumen curvature. This condition has been observed previously by Akyildiz et al. in 2D models of atherosclerotic coronary arteries (17).

Our extensive structural analysis was used to derive a multi-variable nonlinear predictive model that takes into account the individual and combined effect of each risk factor. This model has proved capable of predicting the vulnerability risk of the human atheroma under varying conditions, with full precision in determining whether the cap would rupture or be stable.

This study also presents some limitations that should be acknowledged. First, our models don't include circumferential or axial residual stresses. Ohayon et al. (45) demonstrated that neglecting residual stresses leads to overestimated peak stresses. However, the location of maximal stresses does not seem to shift. Additionally, we did not introduce the effect of the lumen radius in our analysis, which shows a certain degree of influence on plaque vulnerability (39). Lastly, we simulated the presence of blood flow by applying a uniform radial pressure, neglecting the contribution of luminal shear stresses. However, since tensional wall stresses are  $10^3$ - $10^5$  (3-5 orders of magnitude) greater than wall shear stresses, we believe our analysis properly reproduces the vascular stress distributions that reflect the plaque mechanical stability.

In conclusion, the present study provides an analysis of several major morphology and tissue composition factors that play an important role in the background stresses in the atheroma cap, and its combined effect with the presence of a  $\mu$ Calc in the cap tissue. We showed that  $\mu$ Calcs and cap thickness are the two most alarming biomechanical traits that govern the risk of mechanical rupture. Our findings provide supporting evidence that the combination of these risk factors have a synergistic effect on the vulnerability of the atheroma. Certainly, the vulnerability index of caps is greatly enhanced by the presence of even one  $\mu$ Calc, an effect that was not observed when the cap thickness and the  $\mu$ Calc were analyzed in isolation. A  $\mu$ Calc has the potential to transform relatively thick caps into vulnerable ones. The phenotype of biomechanically vulnerable lesions can be described as non-obstructive plaques with softer (lipid-rich) cores and a thin cap with  $\mu$ Calcs. Indeed, the appearance of a  $\mu$ Calc in the cap of an otherwise stable plaque is able to transform it into a vulnerable one.

#### 5 Contribution to the field statement

- The most common underlying cause of acute coronary events is atherosclerosis, which is initiated by
- 416 cholesterol build-up beneath the arterial endothelium and ultimately evolves into an atherosclerotic
- plague, also called atheroma. The rupture of the fibrous cap of a vulnerable plague is associate with
- 418 major clinical outcomes, including myocardial infarction and sudden coronary death. The definition of
- 419 high-risk vulnerable plaque has evolved over time, as pathological and biomechanical studies have
- 420 uncovered multiple factors that determine the stability of an atheroma. We present an extensive
- 421 structural analysis of the individual and combined effect of major biomechanical factors of plaque
- 422 vulnerability and define the phenotypes with higher risk of rupture based on the cap thickness,
- morphology of the lesion, the lipid core stiffness, the blood pressure and the presence of µCalcs. We
- 424 provide evidence that non-obstructive lesions with a thin fibrous cap experience significantly higher
- stresses in the tissue and appear less stable than highly-stenotic, stiff, advanced plaques, especially
- 426 under hypertensive conditions. Additionally, our findings emphasize the importance of assessing the
- potential presence of µCalcs in the cap tissue, as they may transform stable plaques into rupture-prone
- 428 lesions.

414

#### 429 6 Acknowledgments

430 None

#### 431 7 Conflict of Interest

- 432 The authors declare that the research was conducted in the absence of any commercial or financial
- relationships that could be construed as a potential conflict of interest.

#### 434 8 Authors Contribution Statement

- 435 Andrea Corti: Conceptualization, Methodology, Data Curation, Validation, Writing-original
- draft; Annalisa De Paolis: Methodology, Data Curation, Validation; Pnina Grossman:
- 437 Methodology, Data Curation; **Puch A. Dinh**: Methodology, Data Curation; **Elena Aikawa**:
- 438 Supervision, Writing-review & editing, Funding acquisition; **Sheldon Weinbaum**: Supervision,
- Writing-review & editing, Funding acquisition; **Luis Cardoso**: Conceptualization, Methodology,
- 440 Supervision, Writing-review & editing, Funding acquisition.

#### **441 9 Funding**

- 442 NIH grant 1R01HL136431 and 1R16GM145474, NSF grants CMMI-1662970, MRI-2018485, PSC-
- 443 CUNY 64696-00 52.

#### 445 **Bibliography**

444

- 1. Arbab-Zadeh A, Fuster V. From Detecting the Vulnerable Plaque to Managing the Vulnerable Patient: JACC State-of-the-Art Review. J Am Coll Cardiol [Internet]. 2019;74(12):1582–93.
- 448 Available from: https://doi.org/10.1016/j.jacc.2019.07.062
- 449 2. Tomaniak M, Katagiri Y, Modolo R, de Silva R, Khamis RY, Bourantas C V., et al.
- Vulnerable plaques and patients: State-of-the-art. Eur Heart J. 2020;41(31):2997–3004.

- 451 3. Arbab-Zadeh A, Nakano M, Virmani R, Fuster V. Acute coronary events. Circulation.
- 452 2012;125(9):1147–56.
- 453 4. Virmani R, Burke AP, Farb A, Kolodgie FD. Pathology of the Vulnerable Plaque. J Am Coll Cardiol. 2006;47(8 SUPPL.):0–5.
- Virmani R, Kolodgie FD, Burke AP, Farb A, Schwartz SM. Lessons From Sudden Coronary Death. Arterioscler Thromb Vasc Biol. 2000;20(5):1262–75.
- 457 6. Kramer MCA, Rittersma SZH, de Winter RJ, Ladich ER, Fowler DR, Liang YH, et al.
- 458 Relationship of Thrombus Healing to Underlying Plaque Morphology in Sudden Coronary
- 459 Death. J Am Coll Cardiol. 2010;55(2):122–32.
- Fuster V, Moreno PR, Fayad ZA, Corti R, Badimon JJ. Atherothrombosis and high-risk
   plaque: Part I: Evolving concepts. J Am Coll Cardiol [Internet]. 2005;46(6):937–54. Available
   from: http://dx.doi.org/10.1016/j.jacc.2005.03.074
- Varnava AM, Mills PG, Davies MJ. Relationship between coronary artery remodeling and plaque vulnerability. Circulation. 2002;105(8):939–43.
- 465 9. Lendon CL, Davies MJ, Born GVR, Richardson PD. Atherosclerotic plaque caps are locally weakened when macrophages density is increased. Atherosclerosis. 1991;87(1):87–90.
- Underhill HR, Hatsukami TS, Fayad ZA, Fuster V, Yuan C. MRI of carotid atherosclerosis:
   Clinical implications and future directions. Nat Rev Cardiol [Internet]. 2010;7(3):165–73.
- 469 Available from: http://dx.doi.org/10.1038/nrcardio.2009.246
- Virmani R, Narula J, Leon MB, Willerson JT. The vulnerable atherosclerotic plaque. Wiley-Blackwell; 2008. 384 p.
- Virmani R, Kolodgie FD, Burke AP, Finn A V., Gold HK, Tulenko TN, et al. Atherosclerotic
   plaque progression and vulnerability to rupture: Angiogenesis as a source of intraplaque
   hemorrhage. Arterioscler Thromb Vasc Biol. 2005;25(10):2054–61.
- Partida RA, Libby P, Crea F, Jang IK. Plaque erosion: A new in vivo diagnosis and a potential major shift in the management of patients with acute coronary syndromes. Eur Heart J. 2018;39(22):2070–6.
- 478 14. Cheng GC, Loree HM, Kamm RD, Fishbein MC, Lee RT. Distribution of circumferential stress in ruptured and stable atherosclerotic lesions: A structural analysis with histopathological correlation. Circulation. 1993;87(4):1179–87.
- Finet G, Ohayon J, Rioufol G. Biomechanical interaction between cap thickness, lipid core composition and blood pressure in vulnerable coronary plaque: Impact on stability or instability. Coron Artery Dis. 2004;15(1):13–20.
- 484 16. Ohayon J, Finet G, Gharib AM, Herzka DA, Tracqui P, Heroux J, et al. Necrotic core 485 thickness and positive arterial remodeling index: Emergent biomechanical factors for 486 evaluating the risk of plaque rupture. Am J Physiol - Hear Circ Physiol. 2008;295(2):717–27.

- 487 17. Akyildiz AC, Speelman L, Nieuwstadt HA, van Brummelen H, Virmani R, van der Lugt A, et 488 al. Effects of plaque morphology and material properties on peak cap stress in human coronary 489 arteries. Comput Methods Biomech Biomed Engin. 2016;19(7):771–9.
- 490 18. Glagov S. Remodeling 1987 Compensatory enlargement of human atherosclerotic coronary arteries. N Engl J Med. 1971;18:1182–6.
- 492 19. Cardoso L, Weinbaum S. Changing views of the biomechanics of vulnerable plaque rupture: A review. Ann Biomed Eng. 2014;42(2):415–31.
- 494 20. Fu BM, Wright NT. Molecular, Cellular, and Tissue Engineering of the Vascular System
  495 [Internet]. Vol. 1097. 2018. 335 p. Available from: http://link.springer.com/10.1007/978-3496 319-96445-4
- 497 21. Ohayon J, Finet G, Pettigrew R. Biomechanics of coronary atherosclerotic plaque from model to patient. Academic Press; 2020. 633–653 p.
- 499 22. Criqui MH, Denenberg JO, Ix JH, McClelland RL, Wassel CL, Rifkin DE, et al. Calcium
   500 density of coronary artery plaque and risk of incident cardiovascular events. JAMA J Am
   501 Med Assoc. 2014;311(3):271-8.
- Criqui MH, Knox JB, Denenberg JO, Forbang NI, McClelland RL, Novotny TE, et al.
   Coronary Artery Calcium Volume and Density: Potential Interactions and Overall Predictive
   Value: The Multi-Ethnic Study of Atherosclerosis. JACC Cardiovasc Imaging.
   2017;10(8):845–54.
- Rambhia SH, Liang X, Xenos M, Alemu Y, Maldonado N, Kelly A, et al. Microcalcifications increase coronary vulnerable plaque rupture potential: A patient-based micro-ct fluid-structure interaction study. Ann Biomed Eng. 2012;40(7):1443–54.
- Cardoso L, Kelly-Arnold A, Maldonado N, Laudier D, Weinbaum S. Effect of tissue
   properties, shape and orientation of microcalcifications on vulnerable cap stability using
   different hyperelastic constitutive models. J Biomech [Internet]. 2014;47(4):870–7. Available
   from: http://dx.doi.org/10.1016/j.jbiomech.2014.01.010
- Vengrenyuk Y, Carlier S, Xanthos S, Cardoso L, Ganatos P, Virmnani R, et al. A hypothesis for vulnerable plaque rupture due to stress-induced debonding around cellular microcalcifications in thin fibrous caps. Proc Natl Acad Sci U S A. 2006;103(40):14678–83.
- 516 27. Kelly-Arnold A, Maldonado N, Laudier D, Aikawa E, Cardoso L, Weinbaum S. Revised microcalcification hypothesis for fibrous cap rupture in human coronary arteries. Proc Natl Acad Sci U S A. 2013;110(26):10741–6.
- 519 28. Loree HM, Tobias BJ, Gibson LJ, Kamm RD, Small DM, Lee RT. Mechanical properties of model atherosclerotic lesion lipid pools. Arterioscler Thromb. 1994;14(2):230–4.
- 521 29. Maldonado N, Kelly-Arnold A, Cardoso L, Weinbaum S. The explosive growth of small voids 522 in vulnerable cap rupture; cavitation and interfacial debonding. J Biomech. 2013;46(2):396– 523 401.

- 524 30. Maldonado N, Kelly-Arnold A, Vengrenyuk Y, Laudier D, Fallon JT, Virmani R, et al. A
- 525 mechanistic analysis of the role of microcalcifications in atherosclerotic plaque stability:
- 526 potential implications for plaque rupture. Am J Physiol Circ Physiol. 2012;303(5):H619–28.
- 527 31. Maldonado N, Kelly-Arnold A, Laudier D, Weinbaum S, Cardoso L. Imaging and analysis of
- 528 microcalcifications and lipid/necrotic core calcification in fibrous cap atheroma. Int J
- 529 Cardiovasc Imaging. 2015;31(5):1079–87.
- Hutcheson JD, Goettsch C, Bertazzo S, Maldonado N, Ruiz JL, Goh W, et al. Genesis and
- growth of extracellular-vesicle-derived microcalcification in atherosclerotic plaques. 2016;11.
- 532 33. Holzapfel GA, Sommer G, Gasser CT, Regitnig P. Determination of layer-specific mechanical
- properties of human coronary arteries with nonatherosclerotic intimal thickening and related
- constitutive modeling. Am J Physiol Circ Physiol. 2005;289(5):H2048–58.
- 535 34. Gasser TC, Ogden RW, Holzapfel GA. Hyperelastic modelling of arterial layers with
- distributed collagen fibre orientations. J R Soc Interface. 2006;3(6):15–35.
- 537 35. Corti A, De Paolis A, Tarbell J, Cardoso L. Stenting-induced Vasa Vasorum compression and
- subsequent flow resistance: a finite element study. Biomech Model Mechanobiol [Internet].
- 539 2021;20(1):121–33. Available from: https://doi.org/10.1007/s10237-020-01372-x
- 540 36. Volokh KY. Modeling failure of soft anisotropic materials with application to arteries. J Mech
- Behav Biomed Mater [Internet]. 2011;4(8):1582–94. Available from:
- 542 http://dx.doi.org/10.1016/j.jmbbm.2011.01.002
- 543 37. Hutcheson JD, Goettsch C, Bertazzo S, Maldonado N, Ruiz JL, Goh W, et al. Genesis and
- growth of extracellular-vesicle-derived microcalcification in atherosclerotic plaques. Nat
- 545 Mater. 2016;15(3):335–43.
- 546 38. Vengrenyuk Y, Cardoso L, Weinbaum S. Micro-CT based analysis of a new paradigm for
- 547 vulnerable plaque rupture: Cellular microcalcifications in fibrous caps. MCB Mol Cell
- 548 Biomech. 2008;5(1):37–47.
- 549 39. Cilla M, Peña E, Martínez MA. 3D computational parametric analysis of eccentric atheroma
- plaque: Influence of axial and circumferential residual stresses. Biomech Model Mechanobiol.
- 551 2012;11(7):1001–13.
- 552 40. Burke AP, Farb A, Malcom GT, Liang YH, Smialek J, Virmani R. Coronary risk factors and
- plaque morphology in men with coronary disease who died suddenly. N Engl J Med [Internet].
- 554 1997;336(18):1276–1282. Available from: doi: 10.1056/NEJM199705013361802.
- 555 41. Virmani R, Burke AP, Kolodgie FD, Farb A. Pathology of the thin-cap fibroatheroma: A type
- of vulnerable plaque. J Interv Cardiol. 2003;16(3):267–72.
- 557 42. Tanaka A, Imanishi T, Kitabata H, Kubo T, Takarada S, Tanimoto T, et al. Morphology of
- exertion-triggered plaque rupture in patients with acute coronary syndrome: An optical
- coherence tomography study. Circulation. 2008;118(23):2368–73.
- 560 43. Akyildiz AC, Speelman L, Nieuwstadt HA, van Brummelen H, Virmani R, van der Lugt A, et

562		coronary arteries. Comput Methods Biomech Biomed Engin. 2016;19(7):771–9.
563 564 565 566	44.	Maehara A, Mintz GS, Bui AB, Walter OR, Castagna MT, Canos D, et al. Morphologic and angiographic features of coronary plaque rupture detected by intravascular ultrasound. J Am Coll Cardiol [Internet]. 2002;40(5):904–10. Available from: http://dx.doi.org/10.1016/S0735-1097(02)02047-8
567 568 569 570	45.	Ohayon J, Dubreuil O, Tracqui P, Le Floc'h S, Rioufol G, Chalabreysse L, et al. Influence of residual stress/strain on the biomechanical stability of vulnerable coronary plaques: Potential impact for evaluating the risk of plaque rupture. Am J Physiol - Hear Circ Physiol. 2007;293(3).
571		
572		
573		
574		
575		
576		

#### **Supplementary Material**

#### Section 1A. Anatomical features of arterial models

The idealized models (Solidworks, Dassault Systems, v.2018) represent 30mm-long arterial segments and comprise the vascular layers intima, media and adventitia. The arterial layers were modelled as thick-walled cylindrical tubes with thickness values of 0.2, 0.3 and 0.4 mm, respectively (31). Models were conceived to present thickening of the intima layer and an eccentric plaque in agreement with Glagov's morphological and mathematical description of lesion growth (16,18). In particular, the remodeling index (RI) (I), degree of stenosis ( $Stenos_{deg}$ ) (II) and lumen reduction (III) were defined as:

$$RI = \frac{Lu_{area} + Pla_{area} + Int_{area} + Me_{area}}{Lu_{area\_dist} + Int_{area\_dist} + Me_{area\_dist}},$$
 (I)

$$Stenos_{deg} = 100 \left( \frac{Pla_{area}}{Pla_{area} + Lu_{area}} \right), \tag{II}$$

$$Lumen\ reduction = 100 \left(1 - \frac{Lu_{area}}{Lu_{area\_dist}}\right), \tag{III}$$

where  $Lu_{area}$ ,  $Pla_{area}$ ,  $Int_{area}$ ,  $Me_{area}$  are the areas in the diseased section of lumen, plaque, intima, and media, respectively;  $Lu_{area\_dist}$ ,  $Int_{area\_dist}$ ,  $Me_{area\_dist}$  are the areas in the distal, healthy region of lumen, intima and media, respectively. The plaque was designed by inserting a semi-annular lipid core in the intimal layer at the middle of the artery section.

To reproduce the left anterior descending coronary artery geometry for numerical analysis, the sample was scanned with 6.7μm high-resolution microcomputed tomography (HR-μCT). The system energy settings were chosen to increase the contrast between soft tissue and plaque's lipid content and the scan included 8,000 2D slices of 2000 by 2000 in-plane matrix, with 6.7μm isotropic voxel resolution and 8-bit gray levels. We imported the HR-μCT images into Mimics (Materialise, v 21.0) and generated 3D volume meshes for adventitia, media, intima and lipid core based on their different grey color levels. The final geometry comprising the atheroma was cropped to an 18.75-mm long segment with thickness values of 0.2, 0.2 and 0.3 mm for intima, media and adventitia, respectively.

#### Section 1B. Material Properties

The HGO model describes the material response to large deformation using the strain energy function *W* given by (IV):

$$W = C_{10}(\bar{I}_1 - 3) + \frac{k_1}{2k_2} \sum_{i=1}^{N} \left[ exp(k_2 \langle \bar{E}_i^2 \rangle) - 1 \right] + \frac{1}{D} \left( \frac{J^2 - 1}{2} - lnJ \right)$$
 (IV)

602 with,

$$\bar{E}_i \stackrel{\text{def}}{=} \kappa(\bar{I}_1 - 3) + (1 - 3\kappa)(\bar{I}_{4i} - 1),$$
 (V)

where  $C_{I0}$  describes the isotropic behaviour of the non-collagenous matrix of the artery and is related to the shear modulus  $\mu$  of each layer by (VI):

$$C_{10} = \frac{\mu}{2},\tag{VI}$$

606 D is a material constant related to the bulk modulus K of the tissue by (VII):

$$D = \frac{K}{2'}$$
 (VII)

 $k_1$  and  $k_2$  are constants defining the anisotropic nature of the vascular tissue; the parameter κ describes the level of dispersion in the fiber direction;  $\bar{I}_1$  is the first deviatoric strain invariant; J is the elastic volume ratio and  $\bar{I}_{4i} = A_{0i} : \bar{C}$ ,  $A_{0i} = a_{0i} \otimes a_{0i}$  are the invariants of the distortional part of the right Cauchy-Green strain  $\bar{C}$ . Since the collagen fibers are arranged in symmetrical spirals at different angles depending on the considered layer, they are expressed in a cylindrical coordinate system by (VIII):

$$a_{0i} = \begin{bmatrix} 0 \\ \cos \beta_i \\ \sin \beta_i \end{bmatrix}, i = 1,2 \text{ fiber families}$$
(VIII)

where  $\beta_i$  are the directions of two (i = 1, 2) fiber families in the reference configuration, in each of the vascular layers. The constitutive coefficients for each artery layer were derived by curve fitting the average experimental stress–strain curves from Holzapfel et al. (2005) with the HGO model adjusting the parameters  $k_1$  and  $k_2$  by minimizing the squared error between the data and the HGO model (33). The layer-specific values for each material coefficient are listed in **Supplementary Table 1**.

620 Tissue Failure Simulation

605

612

613614

615

616

617

618

619

621

622

623

The hyperelastic failure description proposed by Volokh et al. (34) includes energy limiters to the strain energy density function of the material for modeling failure of soft tissues. In this framework, the strain energy function  $\psi$  is defined as (IX):

$$\psi(\Phi, W) = \frac{\Phi}{m} \left\{ \Gamma\left(\frac{1}{m}, 0\right) - \Gamma\left(\frac{1}{m}, \frac{W^m}{\Phi^m}\right) \right\} - \Phi \eta \left(\frac{W^m}{\Phi^m}\right)^{1/m}, \tag{IX}$$

where W is the strain energy of the undamaged material;  $\Phi$  is the failure energy limiter; m is a material parameter that controls the sharpness of the transition to material instability on the stress strain curve;  $\Gamma$  is the upper incomplete gamma function defined as  $\Gamma(s,x) = \int_x^\infty t^{s-1} \exp(-t) dt$  and  $\eta$  is a damage scalar variable which defines the threshold value for element removal in the model and is given by (X):

$$\eta = \exp\left(-\frac{W}{\Phi}\right)^m, (0 \le \eta \le 1)$$

The values for  $\Phi$ , m and  $\eta$  were chosen to not alter the stress-strain response of the intima from that reported by Holzapfel et al. and to trigger tissue rupture at a Maximal Principal Stress of 545kPa (**Table2**). This value for rupture represents the average UTS reported by Cheng et al. (14) after performing finite element (FE) simulations on 2D geometries of ruptured plaques.

Layer	C <sub>10</sub> (kPa)	D	$k_l$ (kPa)	k <sub>2</sub> ()	K	$\beta_i$ (degrees)	Ф	m	η
Adventitia	3.78	0	1.99	6.36	0.15	67.0			
Media	0.65	0	184.7	17.13	0.25	20.61		\	
Intima	13.95	0	53.72	2.66	0.163	60.3	1	1	0.8897

#### Section1C. Boundary conditions and Loadings

To capture the effect of µCalcs and tissue rupture mechanism, we implemented the sub-modeling Supplementary Table 1. Values of the constitutive coefficients of the HGO model for the three arterial layers intima, media and adventitia and the damage coefficients for the intima.

approach available in Abaqus to maximize the accuracy of the cap stress calculation (27,35). In the case of idealized geometries, we interpolated the solution of the global model onto the first submodel, consisting of an annular section of the center of the lesion with a mesh element size that was two times finer than the global model (**Fig2B of main manuscript**). The more accurate solution from submodel 1 was then used to solve the second submodel. This represents a 1mm x 1mm arc segment from the center of the fibrous cap with a final mesh element size 10 times smaller than the global mesh.

In the case of the human coronary, the global mesh presents a number of mesh elements per thickness similar to the idealized submodel 1. Therefore, submodel 1 of the human model represents already the cap section (**Fig2C of main manuscript**) with a mesh element size reduced by a factor of 10 as compared to the global model. The tissue damage description and the micro-calcification were introduced only at the last submodel. A dynamic quasi-static implicit approach was used to solve the simulations without the failure formulation. In these models we implemented a four-node linear tetrahedron and hybrid formulation mesh (ABAQUS element type C3D4H). At the smallest scale submodel, an explicit analysis was required to couple the custom-made user subroutine VUMULLINS to replicate tissue rupture. A mass scaling factor of 10<sup>5</sup> was used to ensure the quasi-static condition during the entire simulation (kinetic energy < 5% of internal energy). In this analysis, we assigned a 10-node quadratic tetrahedron and modified formulation mesh (ABAQUS element type C3D10M).